ARTICLES

Interface propagation and nucleation phenomena for discontinuous poisoning transitions in surface-reaction models

J. W. Evans and T. R. Ray*
Ames Laboratory and Department of Mathematics, Iowa State University, Ames, Iowa 50011
(Received 25 July 1994)

Here, we consider discontinuous nonequilibrium phase transitions to poisoned or "adsorbing" states in lattice-gas models of surface reactions. Specifically, we examine the monomer or CO-poisoning transition in the Ziff-Gulari-Barshad monomer-dimer reaction model for CO oxidation, modified to include adspecies diffusion. For CO pressures below the poisoning transition, we first characterize the propagation of and fluctuations at an interface between reactive and CO-poisoned states. Here, we utilize ideas from spatial contact models, reaction-diffusion theory, and kinetic roughening theory. Evolution is described by the Kardar-Parisi-Zhang equation, but with the nonlinearity and kinetic surface tension vanishing on approaching the transition. Next, again for CO pressures below the transition, we consider the evolution of a "nucleus" of the reactive state embedded in the CO-poisoned state, now exploiting concepts from epidemic theory. We elucidate the divergence and "sharpening" of the critical size of this nucleus, both approaching the transition and with increasing adspecies diffusion rates. The deviation from mean-field divergence approaching the transition is related to the vanishing of the kinetic surface tension. The sharpening is related to the reduced influence of fluctuations. Throughout this contribution, we focus on providing a unifying framework that can describe both the fluctuation-dominated behavior of the lattice-gas model for low adspecies diffusion rates, and the crossover to the deterministic mean-field behavior for high diffusion rates where the adlayer is well mixed or randomized.

PACS number(s): 05.40.+j, 82.65.Jv, 82.20.Mj

I. INTRODUCTION

Stochastic lattice-gas models have been increasingly applied to describe far-from-equilibrium processes where rates violate detailed balance, and also to describe open systems. These processes include surface reactions which often exhibit *nonequilibrium phase transitions* between reactive steady states and poisoned or "adsorbing" states [1,2]. A detailed understanding is emerging of such continuous or second-order poisoning transitions, and of associated universality issues [3]. However, it is discontinuous or first-order poisoning transitions that are most commonly observed in surface reaction experiments, and which underlie the rich nonlinear dynamical phenomena and spatiotemporal behavior that have generated so much interest in these systems [4]. Thus, here we focus on characterizing the behavior associated with discontinuous poisoning transitions in lattice-gas models for surface reactions. Specifically, here we analyze the Ziff-Gulari-Barshad monomer-dimer reaction model [5] for CO oxidation, modified to incorporate diffusion of both adspecies [6–8]. This model exhibits a discontinuous transition from a reactive steady state to a trivial adsorbing monomer or CO-poisoned state, with increasing monomer or CO pressure [5–8].

The fundamental motivation for lattice-gas modeling of surface reactions is that this approach has the potential to provide a realistic description of fluctuations and correlations which are ignored in traditional mean-field treatments. These fluctuations and correlations result from the adsorption and reaction processes, as well as from adspecies interactions. Indeed most lattice-gas modeling to date has included zero or low adspecies diffusion rates, which has resulted in "anomolously large" fluctuations and correlations generated by the adsorption and reaction processes [2]. We also emphasize that it is these fluctuations which produce or "automatically select" the discontinuous transition in the reaction model, and their large amplitude is responsible for the weak metastability observed in simulation studies [2]. However, in real systems, high diffusion rates for at least some adspecies lead to a randomization of the adlayer (for weak adspecies interactions), quenching the correlations and fluctuations due to adsorption and reaction, and producing the strong metastability (or "bistability") and hysteresis [4]. The latter observations motivate our inclusion and analysis of the effects of adspecies diffusion in the model.

Just as for discontinuous transitions in equilibrium systems, a primary goal of our analysis of corresponding nonequilibrium transitions is the elucidation of associated interface evolution and nucleation phenomena. Clearly,

*Present address: Department of Mathematics, S. E. Missouri State University, Cape Girardeau, MO 63701.

conventional equilibrium free-energy ideas [9] are not applicable for nonequilibrium poisoning transitions, so here we utilize a diverse variety of alternative conceptual tools. We first consider the evolution of planar interfaces between the stable reactive and the CO-poisoned states for CO pressures below the poisoning transition, noting that such propagation is stable only because of the adsorbing character of the "metastable" CO-poisoned state. The behavior of the propagation velocity is elucidated by integrating ideas from spatial contact models (SCM) [10], which provide a paradigm for propagation in the absence of diffusion, with traditional synergetic reaction-diffusion theory of trigger or chemical wave propagation [11]. We also characterize the fluctuations at this "driven" interface applying recently developed theories of kinetic roughening [12], and showing in particular that the Kardar-Parisi-Zhang equation [13] describes evolution below the transition. To address nucleation issues, we consider the growth probability $P_g(N)$ of a reactive patch or "nucleus" of size N embedded in a CO-poisoned background. Again we just consider CO pressures below the transition, where P_g is well defined by virtue of the adsorbing character of the poisoned state, analogous to epidemic theory studies [14–16]. We determine the critical nucleus size N^*, where $P_g(N=N^*)=\frac{1}{2}$, and then characterize in detail the divergence and "sharpening" of N^*, both approaching the transition and with increasing diffusion rates. Here one finds indispensible the insights into interface propagation and fluctuations obtained earlier.

Another goal of our analysis is to elucidate the crossover from fluctuation-dominated behavior for low adspecies diffusion rates to deterministic mean-field behavior for rapid diffusion. Indeed, our model is selected so that the latter behavior is described exactly by mean-field rate equations (for spatially homogeneous states). In the absence of fluctuations, these exhibit bistability [1,2,4,11]. The discontinuous transitions in the lattice-gas model correspond to the equistability point of two such stable solutions [2,17]. In the mean-field theory, this can be determined by introducing a macroscopic spatial inhomogeneity and studying its evolution via appropriate reaction-diffusion equations [2,17]. The associated planar interface propagation and nucleation phenomena are well characterized [11] and elucidate behavior of the entirely analogous phenomena studied in the lattice-gas model.

As indicated above, precise analysis of interface propagation and nucleation phenomena for the reaction model is only possible because of the trivial adsorbing character of the poisoned state. This allows for stable interface propagation below the transition, and for unambiguous determination of growth or extinction of an embedded reactive nucleus. In contrast, for equilibrium discontinuous transitions at nonzero temperatures, one can set up a stable interface only right at the transition where two distinct phases coexist. Away from the transition, one of these states is metastable or unstable, and the interface will consequently break down. Similarly, a precise definition of growth probability is not possible. Further, we note that the complications apparent for equilibrium systems at nonzero temperatures are also present in this nonequilibrium reaction model, either above the poisoning transition or if one introduces nonreactive desorption of CO. Indeed, nonreactive CO desorption in the reaction model is analogous to nonzero temperatures in the equilibrium model [2,18].

The monomer-dimer surface reaction model considered here, and details of its phase diagram, are, for the most part, described in Sec. II. We do, however, leave the description of the specifics of the determination of spinodals to Sec. III. The development of a general theoretical framework for characterizing the propagation of a planar "reactive interface" separating reactive and poisoned states is presented in Sec. IV, and a description of fluctuations at such interfaces is presented in Sec. V. Some basic ideas and results from epidemic theory are presented in Sec. VI to lay the foundation for the following discussion of nucleation phenomena. The key results on critical size scaling are presented in Sec. VII, and are elucidated in terms of the propagation of curved reactive interfaces. The scaling theory for the full size dependence of the growth probability is detailed in Sec. VIII. Finally, some brief conclusions are made in Sec. IX.

II. MONOMER-DIMER REACTION MODEL AND ITS PHASE DIAGRAM

The monomer-dimer surface reaction model mimicking CO oxidation involves adsorption of a monomer species A (corresponding to CO), on single empty sites, adsorption of a dimer species B_2 (corresponding to O_2) on adjacent pairs of empty sites, and reaction of different species adsorbed on adjacent sites [2,5,19]. The impingement rates for A and B_2 are denoted by y_A and y_B, respectively, and are normalized so that $y_A+y_B=1$. Below θ_A and θ_B denote coverages of adsorbed species. The special case of instantaneous reaction in the absence of surface diffusion is referred to as the Ziff-Gulari-Barshad (ZGB) model [5]. Here, we consider this adsorption-limited reaction model on a square lattice and its generalization to include adspecies diffusion. Specifically, we allow both types of adspecies, A and B, to hop to nearest-neighbor unoccupied sites at the rate $h \geq 0$, for *each* possible direction [6–8]. Although it would be more realistic in modeling CO oxidation to include only diffusion of A (corresponding to CO) [20], here we have included diffusion of both species so that the adlayer is randomized in the limit as $h \to \infty$, and the process can be described exactly by mean-field rate equations and reaction-diffusion equations. The nontrivial limit with just rapid diffusion of adsorbed A (but not B) will be described elsewhere [2,21].

Figure 1 shows a schematic of the steady-state behavior of the monomer-dimer model most relevant to this study: (i) a discontinuous transition between a reactive steady state and an A-poisoned adsorbing state at $y_A=y_2(h)$; (ii) metastable extensions of a reactive steady state above y_2 to the spinodal $y_{s+}(h)$, and of the A-poisoned state below y_2 to the spinodal $y_{s-}(h)$; (iii) an ill-defined unstable branch (see Appendix A) joining the spinodal points to complete a van der Waals type loop. This model also exhibits a continuous B-poisoning transi-

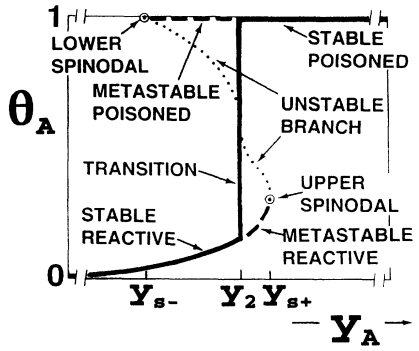

FIG. 1. Schematic of the phase diagram for the monomer-dimer surface reaction. Shown is the discontinuous A-poisoning transition at $y_A = y_2$ and the spinodal points y_{s+} and y_{s-} bounding the existence regions for the metastable reactive and A-poisoned states, respectively. The spinodals are joined by an ill-defined unstable branch which is dependent on system size.

tion at $y_A = y_1(h)$, where $y_1 < y_2$. Simulations [6,15] suggest that y_1 decreases from 0.3907 to zero as h increases from zero to about 3. Many studies have considered universality issues associated with the continuous transition [3,15]. However, as noted above, in this study we focus exclusively on behavior associated with the first-order transition. Several determinations of y_2 via simulation starting from an empty lattice have been corrupted [7,20,22] by the tendency of the system to remain in a metastable reactive state for $y_2 < y_A < y_{s+}$. The situation is exacerbated for $h > 0$, where the range of metastability, and the lifetime of the metastable state, increase dramatically [2,17] with h. (This increase in the lifetime should be expected quite generally [23] since one must recover bistable mean-field behavior as $h \to \infty$.) However, these difficulties can be avoided by seeding the system with a large domain of the poisoned phase [5], by using techniques of epidemic analysis [16], or by using the "constant coverage" (CC) ensemble simulation technique [24] (see Appendix A). The values for y_2 in Table I are determined by the CC technique [24], with the $h \to \infty$ limit determined separately by an appropriate mean-field reaction-diffusion equation analysis [1,8].

The above discussion has implicitly assumed that the spinodals "exist," i.e., are in some sense well defined, and can be suitably determined. Just as in equilibrium theory, and as is already evident from the above discussion, one expects that the spinodals will at least play an important conceptual role [9]. For example, traditionally, the kinetics would be elucidated in terms of nucleation phenomena only for pressures in the "metastable window" that surrounds the discontinuous transition and is bounded by the spinodals. Indeed, this fact in part motivates our analysis of nucleation phenomena in this contribution. However, from studies of discontinuous equilibrium transitions, one knows that the issue of existence of spinodals is nontrivial. It should also be emphasized that the precise characterization of interface propagation and nucleation phenomena presented below actually does not rely on their existence. For these reasons, we delay the discussion of spinodals to Sec. III.

TABLE I. Transition and spinodal locations, and critical size scaling exponents for various h. ϕ(CC) [$\phi(P_g = \frac{1}{2})$] was estimated from a CC-ensemble analysis (from P_g vs N) with uncertainty ± 0.05 (± 0.1). $h = \infty$ mean-field values [8] are also shown.

h	y_2	y_{s-}	y_{s+}	ϕ (CC)	$\phi(P_g = \frac{1}{2})$
0	0.5256	0.495	0.529	1.33	1.3
$\frac{3}{8}$	0.5522	0.44	0.564	1.46	1.6
1	0.5645	0.38	0.583	1.56	1.7
4	0.5794	0.23	0.61	1.72	1.9
∞	0.595	0	$\frac{2}{3}$	2	2

III. DETERMINATION OF SPINODAL POINTS

In equilibrium theory, "pseudospinodal" points have been defined by suitable analytic extension of unique stable states [25], an approach that could also be applied to the monomer-dimer reaction model [26]. Spinodals have also been extracted from the behavior of coarse-grained free energies or related quantities determined from the Hamiltonian. However, such spinodal locations depend on the introduced coarse-graining length scale, prompting the conclusion that spinodals are ill defined [9]. One difference between the equilibrium studies and the reaction models is that only the latter have a unique "intrinsic dynamics." (Prescription of the Hamiltonian does not uniquely determine a dynamics for equilibrium models.) Thus, we naturally utilize the intrinsic dynamics in the studies below of spinodals in reaction models [26]. Another distinguishing feature of our reaction model is that by increasing the adspecies hop rate h, one can cross over to the $h \to \infty$ mean-field limit where the spinodals are precisely defined.

We begin with a brief discussion of the upper spinodal y_{s+}. Here we determine at least effective values of y_{s+} from analysis of scaling of the poisoning kinetics for y_A above y_{s+}. Specifically, one fits the kinetics to the form $\theta_A \sim K_+[(y_A - y_{s+})t]$, regarding y_{s+} as a free parameter [26] (see Fig. 2). This scaling is well satisfied (for h not too large [27]), and is very sensitive to the choice of y_{s+}. This leads to precise determination of the latter, which is clearly distinct from y_2 (see Table I). Alternatively, a pseudospinodal value for y_{s+} can be determined from analytic extension of the reactive steady state above y_2 to a point where it becomes singular [26], the resulting value agreeing reasonably with the above kinetic estimate for $h = 0$. Yet another alternative is to determine y_{s+} from the CC technique [24], but this presumably leads to system size dependent values.

Determination of the location of the lower spinodal y_{s-} is even more problematic (for $h < \infty$). Clearly the pseudospinodal approach of analytic extension of the poisoned state below the transition cannot be applied directly to determine y_{s-} (since the poisoned state is a trivial adsorbing state). However, introducing into the model nonreactive desorption of adspecies A with small

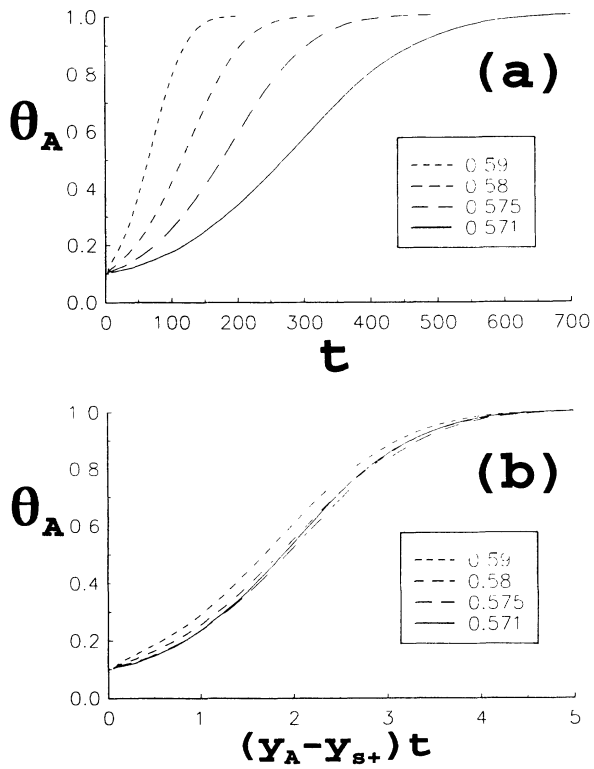

FIG. 2. (a) Reaction kinetics for $h=\frac{3}{8}$ for evolution from an empty lattice to an A-poisoned state for various $y_A > y_{s+}$ (as indicated). (b) Scaled data using $y_{s+}=0.564$; the collapse using 0.563 or 0.566 for y_{s+} is noticeably worse.

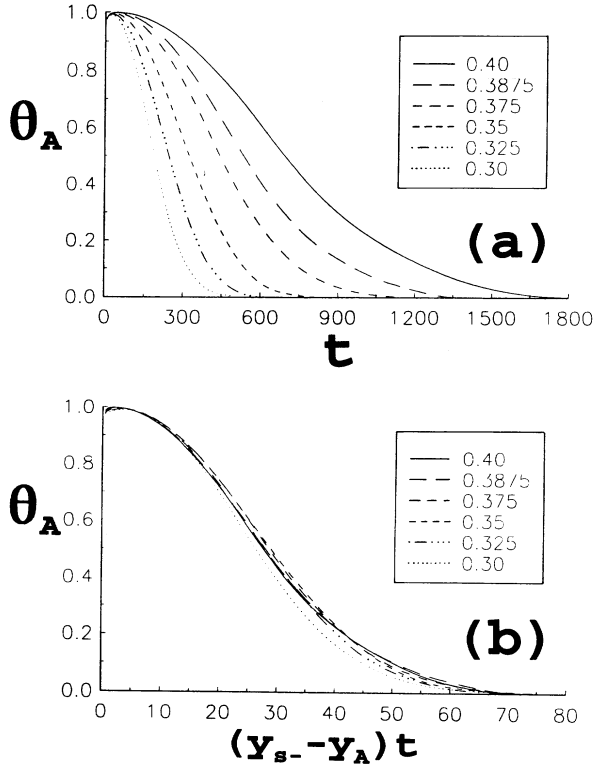

FIG. 3. (a) Reaction kinetics for $h=\frac{3}{8}$ for evolution from a near-A-poisoned state with initial $\theta_A=0.95$ to the reactive steady state for various $y_A < y_{s-}$ (as indicated). (b) Scaled data using $y_{s-}=0.44$; the collapse using 0.43 or 0.45 for y_{s-} is noticeably worse.

rate $d>0$ preserves the discontinuous transition and creates a nontrivial stable steady state (with $\theta_A<1$) above the transition [2,18]. This state could be analytically extended below the transition to determine $y_{s-}(d>0)$, and then finally one must take the limit $d\to 0$. However, more practically, we find that effective values of y_{s-} can be determined reasonably accurately (analogous to y_{s+}) from the kinetics of evolution from a near-A-poisoned state for y_A below y_{s-}. We describe this kinetics by a scaled form, $\theta_A \sim K_-[(y_{s-}-y_A)t]$, regarding y_- as a fitting parameter (see Fig. 3). Specifically, in these studies, an 800×800 lattice is initially randomly filled with A to $\theta_A=0.95$ or 0.97. The objective here is to create a near-A-poisoned surface, with the constraint that the initial state must contain a substantial number of empty pairs to avoid large fluctuations in the kinetics. (Most isolated empty sites will be quickly filled with A, causing θ_A to initially increase much closer to unity.) Results for y_{s-} are insensitive to the choice of initial $\theta_A \geq 0.95$, and clearly distinct from y_2 (see Table I).

Finally, we note that in approximate "dynamic cluster" treatments of the rate equations for these models [19,26,28], and in the exact rate equations for the $h\to\infty$ mean-field limit, y_{s+} corresponds to a saddle-node bifurcation [29] (for all $d\geq 0$). In contrast, y_{s-} corresponds to a transcritical bifurcation [29] (for $d=0$), only being converted to a saddle-node bifurcation with the inclusion of nonreactive A desorption ($d>0$). For $h<\infty$, the estimated positions of the spinodals generally vary strongly with the order of the approximation. Corresponding estimates of the location of the transition y_2 can only be obtained after analysis of chemical wave propagation in approximations to inhomogeneous versions of the rate equations [30].

IV. PROPAGATION VELOCITY OF A PLANAR REACTION INTERFACE

Now we consider in some detail the propagation of (on average) planar interfaces separating the metastable A-poisoned state and the reactive steady state (see Fig. 4). Unless otherwise stated, the interface will be aligned with a principal axis direction of the square lattice of adsorption sites. We necessarily restrict our analysis to y_A below the A-poisoning transition y_2, where the interface is stable, and set $\Delta=y_2-y_A\geq 0$. Since the reactive state is the only stable state for $\Delta>0$, one expects that it will displace the A-poisoned state, resulting in a propagation velocity $V_p=V_p(\Delta)>0$, say, normal to the interface. It is also clear that V_p must vanish as $\Delta\to 0$, where the two states become equistable, so, in general, one writes $V_p\sim\Delta^\gamma$ as $\Delta\to 0$, with $\gamma>0$.

First we consider in detail the vanishing of V_p at the

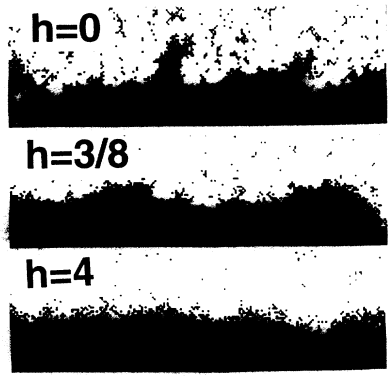

FIG. 4. Snapshots of a portion (200 lattice spacings wide) of the interface between reactive and poisoned states for $\Delta \approx 0$ and for various h. Only A-filled sites are shown.

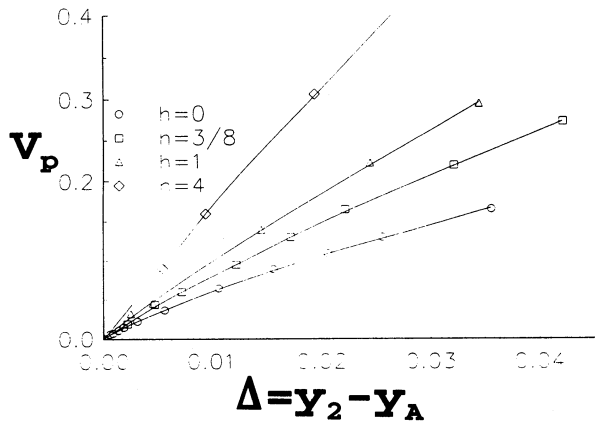

FIG. 5. Vanishing of the planar interface propagation velocity V_p approaching the transition $\Delta \to 0$ for various values of h (shown). The y_2 values (see Table I) used to determine $\Delta = y_2 - y_A$ were determined independently from a CC-ensemble analysis.

transition (for fixed $h < \infty$). The possibility that V_p could vanish nonlinearly, corresponding to $\gamma \neq 1$, should not be immediately discounted. One perspective on this issue comes from the realization that V_p must correspond to the asymptotic expansion velocity of a large surviving reactive patch embedded in an A-poisoned background. Then, as we shall see in Sec. V, γ can be determined from standard epidemic exponents [16] as $\nu(2-\eta-\delta)/2$. The latter quantity is not trivially unity, since the individual exponents are nontrivial and depend on model parameters [16] such as h. For another perspective, note that the interface between the (metastable) reactive state and the (stable) A-poisoned state is unstable above the transition, since the metastable reactive state will eventually poison. Consequently, V_p is ill defined for $\Delta < 0$. Thus, it is not guaranteed that V_p can be analytically extended from $\Delta > 0$ to $\Delta < 0$, which would imply that $\gamma = 1$. On the other hand, the existence of a metastable reactive state above the transition, which allows the possibility of establishing at least transient interface propagation with $V_p < 0$, does suggest that $\gamma = 1$. Finally, we note that it is at least clear that $\gamma \to 1$ when $h \to \infty$. In that limit, interface propagation can be described exactly by mean-field reaction-diffusion equations [2,4,8,11,17]. Here, one finds that interface propagation is stable on both sides of the equistability point (corresponding to $\Delta = 0$) and that V_p vanishes linearly with Δ.

We now report on some simulation results for the behavior of V_p approaching the transition (see Fig. 5). One does indeed find that $V_p \to 0$ as $y_A \to y_2$ (or $\Delta \to 0$), where here y_2 is determined *independently* of a CC-ensemble [24] analysis. From a different perspective, determination of the pressure at which V_p vanishes provides an accurate and efficient method for determination of y_2, which avoids the above mentioned problems with metastability. One expects that the case $h = 0$ will provide the most demanding test of whether γ deviates from unity (recalling that at least $\gamma \to 1$ when $h \to \infty$). The data in Table II are fit by $\gamma = 0.93 \pm 0.1$, strongly suggesting that $\gamma = 1$. V_p data for $h > 0$ are even more convincingly fit by $\gamma = 1$. This strongly suggests that $\gamma(h) = 1$, for all $h \geq 0$, and implies a new scaling relation for epidemic exponents [16]. See Sec. V for further discussion. This result that $\gamma(h) = 1$, for all $h \geq 0$, will be important for our analysis of nucleation phenomena in Sec. VII.

We now continue our analysis of the behavior of the propagation velocity, focusing more on the dependence of V_p on h. Simulation results indicate a monotonic increase of V_p with h, for fixed Δ, specifically from $V_p = 0(1)$, for $h = 0$, to $V_p \sim Ah^{1/2}$, as $h \to \infty$. We suggest that a useful paradigm for propagation in the $h = 0$ diffusionless regime is provided by SCM [10]. These are models for the spread of information or disease by direct contact between neighbors (see Appendix B). Somewhat analogously, in our reaction model for $h = 0$, the coupling to spatial degrees of freedom is a consequence of the reaction of species of different types on adjacent sites (and also of the adjacent empty site adsorption requirement for dimers). The $h \to \infty$ behavior is a consequence of the fact that propagation in this regime is described exactly by mean-field reaction-diffusion equations, where characteristic lengths and velocities scale like the square root of the diffusion coefficient. In fact, analysis of the appropriate equations for our model (see Appendix C) leads to a precise determination of the prefactor A and its dependence on Δ.

TABLE II. Vanishing of V_p for y_A approaching the transition at $y_2 = 0.525\,60$ for $h = 0$. The uncertainty in V_p values is ± 0.0005.

V_p	0.127	0.105	0.087	0.064	0.0355	0.0205	0.0140	0.0100	0.0060
y_A	0.500	0.505	0.510	0.515	0.5200	0.5225	0.523 75	0.524 25	0.524 75

For a more complete elucidation of $h=0$ behavior and the crossover to the $h\to\infty$ regime, it is instructive to consider the following broader class of reaction models. Suppose that reaction can occur between adsorbed A and B separated by l lattice vectors with relative probabilities $p(l)$. Let $l_r^2=\Sigma l^2 p(l)$ denote the variance of this "contact distribution" [10]. Reaction rates need not be infinite here. Also, adspecies hopping at rate h is included as above. Further, we assume that the influence of the surface reaction is described by some pseudo-first-order rate constant k. This would just correspond to the adsorption rate in the case of instantaneous reaction or, more generally, be determined by the rate limiting step. Thus, the characteristic time scale is given by $\tau_c=k^{-1}$. Both the diffusion length $l_d=(h\tau_c)^{1/2}$ and the contact or reaction range l_r provide contributions to the characteristic length l_c. Combining dimensional arguments with the Δ dependence of V_p mentioned above, one writes

$$V_p\sim(l_c/\tau_c)\Delta^\gamma \ . \tag{1}$$

Thus, one has $V_p\sim kl_r\Delta^\gamma$ when $h=0$, and $V_p\sim(hk)^{1/2}\Delta^\gamma$ as $h\to\infty$. We believe that $\gamma=1$ for all h, and certainly $\gamma\to1$ as $h\to\infty$. Interpolation between these regimes might be based on simple "diffusion approximation" ideas for SCM [10], where one converts direct reaction terms into a diffusionlike form assuming weakly varying concentrations over a range l_r (valid at least for $h\gg1$). This suggests an interpolation for l_c between the $h=0$ and $h\to\infty$ regimes of the form $l_c^2\approx cl_r^2+l_d^2$ (see Appendix B).

In the reaction model analyzed above, one has $k=1$ and $l_r=1$, and obtains an interpolation formula for V_p of the form

$$V_p\approx A(B+h)^{1/2} \text{ for fixed } \Delta \ . \tag{2}$$

We find that this form reasonably fits the data for fixed Δ, even when A is not regarded as a fitting parameter, but determined exactly from the mean-field reaction-diffusion equations as described above (see Appendix C). For example, when $\Delta=0.015$, one finds that the variation $V_p=0.086$, 0.114, 0.143, 0.241, 0.385, for $h=0$, 3/8, 1, 4, 16, respectively, is fit reasonably by the mean-field value of $A=0.091$, and choosing $B\approx1.2$.

The above analysis of the behavior of the propagation velocity V_p normal to the interface applies exclusively to planar interfaces aligned with the principal axis direction. It is also instructive to determine whether the V_p depends on the orientation of the propagating planar interface. Certainly V_p is *independent* of orientation in the $h\to\infty$ limit, since the rotational symmetry of the underlying square lattice implies that the macroscopic diffusion tensor appearing in the reaction-diffusion equations must be isotropic. One expects that any anisotropy for $h<\infty$, associated with the underlying square lattice, should be strongest in the absence of diffusion. Thus, for $h=0$, we compare V_p for propagation of interfaces aligned in the (1,0) direction, and tilted at 45° in the (1,1) direction (for the same y_A). We find no anisotropy in V_p to within the statistical uncertainty (2%) of our measurements, e.g., $V_p=0.1268\pm0.0020$ for the (1,0) direction, and $V_p=0.1266\pm0.0020$ for the (1,1) direction, when $y_A=0.5$ (and $h=0$). We expect that, just as in the simple Eden growth model [31], anisotropy might exist, but would be very weak. This observation will be exploited in our analysis in Sec. V of fluctuations at the propagating interface.

V. FLUCTUATIONS AT A PLANAR REACTION INTERFACE: KPZ EVOLUTION

Next we characterize the fluctuations at (on average) planar interfaces between reactive and A-poisoned states for $\Delta=y_2-y_A\geq0$. Examination of Fig. 4 reveals large intrinsic local fluctuations for small h. These are largely independent of time t and small Δ, but are quickly quenched with increasing h. Based on general ideas associated with the kinetic roughening of driven interfaces [12], the total interface width or "fluctuation length" ξ is thus naturally written as $\xi^2\approx\xi_i^2+\xi_0^2$ (cf. Ref. [32]). Here, ξ_i is associated with the above mentioned intrinsic local fluctuations, and ξ_0 with long-wavelength nonlocal fluctuations. The latter grow indefinitely with time, and ultimately dominate the ξ_i (for an infinite system). Below we give a more detailed characterization of the evolution of this fluctuating interface, and specifically of the growth of ξ_0.

The strategy is to develop a stochastic evolution equation providing a coarse-grained description of the propagation of an on-average planar interface with "height" in the direction (1,0) of $h=h(x)$ at "lateral position" x in the (0,1) direction (see Fig. 6). Then $\partial h/\partial t=V_{(1,0)}$ gives the *projection* of the propagation velocity in the direction of the principal axis (1,0). In general, this is expected to depend on the tilt of the interface $\partial h/\partial x$, the curvature, and, thus, on $\partial^2 h/\partial x^2$, as well as on higher derivatives. Consequently, assuming small mean local slopes, one naturally invokes the Kardar-Parisi-Zhang (KPZ) [12,13] type expansion

$$\begin{aligned}\partial h/\partial t&=V_{(1,0)}\\&=V_0+\tfrac{1}{2}\lambda(\partial h/\partial x)^2+\kappa\partial^2 h/\partial x^2+\cdots+\zeta(x) \ ,\end{aligned} \tag{3}$$

where $\zeta(x)$ denotes a δ-function-correlated noise term that generates the fluctuations, and odd powers of gradients are absent in this expansion by symmetry.

We now exploit a key observation from Sec. IV that the propagation velocity *normal* to the interface is effectively independent of orientation and equals V_p. Thus for an on-average planar interface with mean inclination $\langle\partial h/\partial x\rangle$, a simple Pythagorean construction yields

$$\begin{aligned}\langle V_{(1,0)}\rangle&=V_p[1+\langle\partial h/\partial x\rangle^2]^{1/2}\\&\approx V_p+\tfrac{1}{2}V_p\langle\partial h/\partial x\rangle^2 \ .\end{aligned} \tag{4}$$

When compared with an approximation to (3) neglecting fluctuations in $\partial h/\partial x$, specifically,

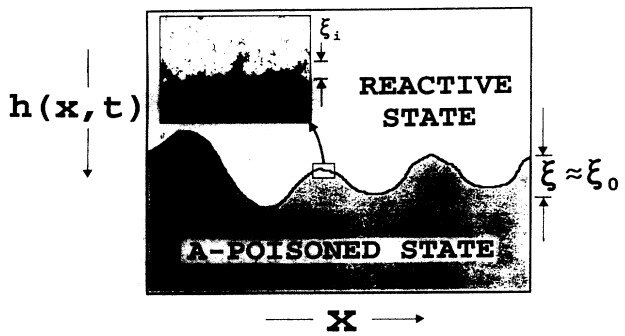

FIG. 6. Schematic of fluctuations in a coarse-grained picture of reactive interface evolution.

$$\langle V_{(1,0)} \rangle \approx V_0 + \tfrac{1}{2}\lambda \langle (\partial h/\partial x)^2 \rangle \approx V_0 + \tfrac{1}{2}\lambda \langle \partial h/\partial x \rangle^2 , \quad (5)$$

one finds that $V_0 \approx V_p$, and $\lambda \approx V_p$. One thus concludes that the KPZ nonlinearity is necessarily present for driven interface propagation below the transition $\Delta > 0$, and that this nonlinearity necessarily vanishes as one approaches the transition where the interface is stationary. The latter feature is, of course, true for any nondriven, or equilibrium, situation, where the propagation velocity is zero for all interface orientations. As an aside, we note that an analysis of the Eden model for interface or cell growth [31], where in addition the propagation velocity is almost independent of interface orientation, provided the original motivation for the KPZ equation [13].

Next we consider other terms in the evolution equation (3). At the quadratic level, the presence of a nonlinear term requires an additional linear term, $\kappa \partial^2 h/\partial x^2$, with $\kappa > 0$ to stabilize interface propagation [33]. This term describes the curvature dependence of the propagation velocity which, e.g., efficiently damps out sinusoidal perturbations of the interface. Thus, κ is naturally identified as a *kinetic surface tension*. (We note that the value of κ depends on the length scale of observation [34].) We do not discuss in detail the implicit higher-order terms in Eq. (3) (which describe, for example, weaker stabilizing effects), since the asymptotic roughening is controlled by the quadratic terms for $\Delta > 0$.

In general, for the stochastic evolution of driven interfaces along a strip of width L, one expects the long-wavelength fluctuations to scale like [12]

$$\xi_0 \sim L^{\alpha} f(t/L^z) , \quad (6)$$

where $f(x) \sim x^{\beta}$ for $x \ll 1$ and $f(x) \to 1$ for $x \gg 1$, with $z = \alpha/\beta$. Thus, for an infinite system $L \to \infty$, one has $\xi_0 \sim t^{\beta}$, as $t \to \infty$. For reactive interface propagation below the transition $\Delta > 0$, where $\lambda > 0$ and $\kappa > 0$, the exponents must assume KPZ values [12,13] of $\beta = \frac{1}{3}$, $\alpha = \frac{1}{2}$, and $z = \frac{3}{2}$.

More generally, kinetic roughening theory provides the following picture of evolution of the driven reactive interface for $\Delta > 0$. The propagating interface quickly equilibrates locally with V_p approaching its asymptotic value like [35] $t^{-2/3}$, and local structure being dominated by intrinsic fluctuations for small h. However, it will continue to roughen globally according to KPZ dynamics with $\beta = \frac{1}{3}$ and $\alpha = \frac{1}{2}$ when $\Delta > 0$.

Finally, we comment on behavior approaching the transition $\Delta \to 0$, where $V_p = 0$ and the quadratic nonlinearity in the evolution equation vanishes. This limit is of particular relevance for our study below of nucleation phenomena. If the kinetic surface tension κ were to remain nonzero, then the KPZ equation would reduce to the linear Edwards-Wilkinson equation [12] for which $\beta = \frac{1}{4}$ and $\alpha = \frac{1}{2}$. However, for these reaction models, we find that $\kappa \to 0$ as $\Delta \to 0$, a feature which is, in fact, shown most clearly from our nucleation studies below. One thus expects that $\beta > \frac{1}{4}$ when $\Delta = 0$, the actual value being determined by the lowest-order terms appearing in the evolution equation. Higher values of β correspond to higher-order dominant terms, or weaker stabilizing effects. (There are stabilizing mechanisms weaker than the kinetic surface tension.) The maximum value of β is $\frac{1}{2}$, corresponding to the lack of any stabilizing effects [12]. From direct simulations of roughening at the transition where $\Delta = 0$, we find [36] $\beta = \beta^* \approx 0.3$ (and $z^* > 1$), clearly indicating the presence of weak stabilizing effects. A detailed discussion of these and related studies will be presented in a separate communication [36].

It is appropriate to compare this behavior with that of interface propagation in the monomer (A)-monomer (B) reaction model [37]. Here the stable steady state is A-poisoned (B poisoned) for $y_A > y_B$ ($y_A < y_B$), producing a discontinuous transition at $y_A = y_B$. For $y_A = y_B$, the interface between the A- and B-poisoned states is in equilibrium, so trivially the KPZ nonlinearity in the stochastic evolution equation must be absent. However, simulations [37] (for random adsorption) show that $\beta = \frac{1}{2}$, so no kinetic surface tension or even any weaker stabilizing mechanisms are present. This difference from the monomer-dimer model should not be surprising, since, e.g., the "trivial" transition in the monomer-monomer model does not display any metastability in the sense of Sec. III.

VI. EPIDEMIC THEORY FOR REACTION MODELS

Here we review and refine some relevant concepts and ideas from epidemic theory [14–16] that apply to "nucleation phenomena" in the reaction models under consideration. Specifically, we consider the evolution for $\Delta = y_2 - y_A > 0$ of a "reaction epidemic" initiated by embedding a roughly square patch of N empty sites in an A-poisoned background. Basic quantities of interest include the survival probability $P_s(N,t)$ and the average number of empty sites, $N_e(N,t)$, at time t, where traditionally the latter quantity is averaged over all (surviving and extinct) epidemic trials. Traditionally, epidemic theory regards N as fixed and analyzes the variation of these quantities with t and Δ. For fixed N, one expects the scaling forms [14–16]

$$P_s(t) \sim t^{-\delta} \phi(\Delta t^{1/\nu}) \text{ and } N_e(t) \sim t^{\eta} f(\Delta t^{1/\nu}) , \quad (7)$$

where δ, η, and ν are nontrivial scaling exponents. Since

there are no long range correlations at the discontinuous transition which could "wash out" dependence on model details, these exponents will depend on model parameters, i.e., there is *no* universality [16].

Since a reactive state rather than the A-poisoned state is the stable steady state for $\Delta = y_2 - y_A > 0$, there is a nonzero (asymptotic) growth probability, $P_g(N) = P_s(N, t \to \infty) > 0$. This corresponds to the nonpoisoned patch surviving indefinitely and thus spreading the reactive steady state across the surface. Consequently, one must have [14–16] $\phi(x) \sim x^{\nu\delta}$ as $x \to \infty$, which implies that $P_g \sim \Delta^{\nu\delta}$ as $\Delta \to 0$.

One also expects that surviving epidemics are, on average, circular, and expand with asymptotically constant velocity. This asymptotic velocity must equal V_p, since the perimeter of a surviving epidemic becomes locally planar. Consequently, one must have $N_e \sim P_g (V_p t)^2$, from which it follows that $f(x) \sim x^{\nu(2-\eta)}$ and, therefore, that $V_p^2 \sim \Delta^{\nu(2-\eta-\delta)}$. Since $V_p \sim \Delta^{\gamma}$ from Sec. IV, one finally obtains [16] $\gamma = \nu(2-\eta-\delta)/2$, which is the relation mentioned in Sec. IV connecting γ with "standard" epidemic exponents. Consequently, the observation that $\gamma = 1$ provides a new and nontrivial scaling relation for these exponents.

To determine $\delta = \delta(h)$, one naturally analyzes the behavior of $P_s \sim t^{-\delta}$ when $\Delta = 0$ (see Fig. 7). One finds that [16] $\delta(h=0) = 3.7 \pm 0.3$, but that δ increases quickly with h, making it difficult to determine precisely, except for very small h. For example, only by running $\sim 10^7$ epidemic trials are we able to determine that $\delta(h = \frac{3}{8}) \approx 12$. The origin of this behavior is clear. For $h \gg 0$, the N initially empty sites are quickly dispersed by diffusion, and since only A can absorb on isolated empty sites (with rate y_A), it follows that $P_s \sim 1 - [1 - \exp(-y_A t)]^N$ as $h \to \infty$ (for fixed t). Thus, for $h \gg 0$, one expects that P_s will be very small upon reaching the asymptotic regime.

We emphasize that even for $h = 0$, δ is very large compared with the directed percolation value [14,15] of 0.45, so there are relatively few surviving epidemics. It seems clear that the asymptotic behavior of N_e will be driven by this feature and, thus, will be particularly difficult to determine. Furthermore, the value of η will reflect the large value of δ. These considerations also suggest that it is more appropriate to consider the average number of

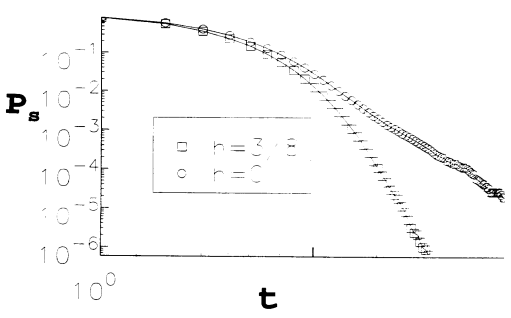

FIG. 7. Epidemic survival probability P_s vs t at the transition $\Delta = 0$ starting with a 2×1 empty patch in an A-poisoned background. Behavior is shown for $h = 0$ and $h = \frac{3}{8}$.

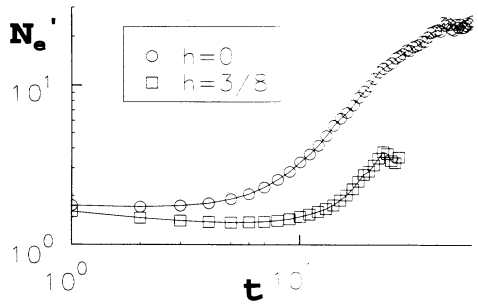

FIG. 8. Average number of empty sites in *surviving* epidemics $N_e' = N_e / P_s$ vs t at the transition $\Delta = 0$, starting with a 2×1 empty patch. Behavior is shown for $h = 0$ and $h = \frac{3}{8}$.

empty sites per surviving epidemic, $N_e' = N_e / P_e \sim t^{\eta'}$, when $\Delta = 0$ (see Fig. 8). It then follows that $\eta = -\delta + \eta'$, with $\eta' \geq 0$, so $\gamma = \nu(1-\eta')/2$. We obtain $0 \leq \eta' \leq 0.6$ for $h = 0$ from the behavior of N_e' for the temporal range $t \geq 25$ where growth apparently occurs at a lower rate. This slower asymptotic growth is not readily discernable directly from N_e behavior, and so corresponding previous direct estimates of η were inaccurate [16,38]. Estimation of η' for $h > 0$ is more difficult, e.g., even our $h = \frac{3}{8}$ data are inadequate for this purpose. Finally, we note that the requirement that $\gamma = 1$ and a previous estimate [16] of $\nu = 0.9 \pm 0.3$ for $h = 0$ suggest that the actual value of η' is somewhat smaller than 0.6.

VII. NUCLEATION PHENOMENA: CRITICAL SIZE BEHAVIOR

To elucidate the nucleation of the reactive steady state from a near-A-poisoned state below the transition, where $\Delta = y_2 - y_A > 0$, one naturally attempts to characterize the evolution of a reactive (or empty) patch embedded in an A-poisoned background, as described in Sec. VI. However, in contrast to traditional analyses of epidemic theory, here one naturally focuses on the dependence of the patch or nucleus growth probability P_g on the initial size N of the embedded patch (at fixed Δ). From this dependence, one can extract the quantity of primary interest, critical size N^*, for which the embedded patch or nucleus has an equal chance of growth and survival or shrinkage and extinction, i.e., $P_g(N = N^*) = \frac{1}{2}$. It is clear that the critical size N^* should diverge approaching $\Delta \to 0$, where the driving force for the reactive state to displace the poisoned state vanishes. Thus, also invoking dimensional arguments, one naturally writes

$$N^* \sim l_c^2 \Delta^{-\phi} \text{ as } \Delta \to 0 , \tag{8}$$

with a nontrivial exponent $\phi > 0$. Here we discuss the dependence of N^* on Δ and h, embodied in this relation, leaving an analysis of the full dependence of P_g on N to Sec. VIII.

Table III summarizes our results for N^* determined from the N dependence of P_g via $P_g(N = N^*) = \frac{1}{2}$. Here we also utilize a different technique to more directly and

TABLE III. Estimates of critical sizes N^* chosen as the initial number of empty sites, and determined from the relation $P_g(N^*)=\frac{1}{2}$. For $h=\frac{3}{8}$, we also obtain $N^*=690$ for $y_A=0.5463$, and $N^*=175$ for $y_A=0.5395$.

			$h=0$		
N^*	840	310	137	79	42
y_A	0.523	0.520	0.515	0.510	0.500
			$h=\frac{3}{8}$		
N^*	900	350	97		
y_A	0.5463	0.5411	0.525		
			$h=4$		
N^*	4360	1430	460		
y_A	0.573	0.568	0.551		

accurately determine N^*. This technique, described in detail in Appendix A, exploits a special feature of the CC-ensemble approach [24] to automatically select critical sized nuclei. Corresponding results are shown in Table IV. First, we consider the divergence of N^* as $\Delta\to 0$. From both techniques, one finds a consistent trend in values for the nonuniversal exponent $\phi=\phi(h)$ (see Table I). Clearly, $\phi(h)<2$ for $h<\infty$, and $\phi(h)$ increases monotonically toward the mean-field value of $\phi=2$ (see below) as $h\to\infty$. Next, we consider the variation of N^* with increasing h (for fixed Δ). Interpolation of the precise CC-ensemble data for N^* (see Table V) reveals a quasilinear variation $N^*\approx E(F+h)$. This is expected from the relation $l_c^2\approx cl_r^2+l_d^2$ proposed in Sec. IV, and is consistent with mean-field behavior $N^*\sim Eh$ as $h\to\infty$, where $E\sim e\Delta^{-2}$ as $\Delta\to 0$ (see below and Appendix C). Indeed, the data of Table V are fit roughly using independently determined exact mean-field values of $E=95$, 265, 1680 for $\Delta=0.03$, 0.0175, 0.0066, and choosing $F=1$, 0.5, 0.2, respectively. These E values were obtained from an analysis of the appropriate mean-field reaction-diffusion equations for a circular patch of the reactive state embedded in an A-poisoned background (see Appendix C).

We now elucidate the observed critical size behavior, exploiting some observations about the propagation of curved interfaces between reactive and A-poisoned states, and also utilizing some corresponding mean-field results. Consider again a circular reactive patch of radius R, embedded in an A-poisoned background for $\Delta>0$. From the KPZ equation [13], one finds that the interface propagation velocity is modified by curvature and, furthermore, the correction is given by κ/R as $R\to\infty$. Here, we write the KPZ kinetic surface tension as $\kappa\sim\Delta^{\sigma}l_c^2/\tau_c$ for small Δ, based on dimensional arguments and allowing for possible Δ dependence (if $\sigma\neq 0$). Thus the mean outward propagation velocity $V(R)$ of this patch should satisfy

$$V_p-V(R)\sim\kappa/R \text{ for large } R\gg l_c \ . \tag{9}$$

Now, if R^* denotes the critical radius satisfying $N^*=\pi(R^*)^2$, then one has $V(R^*)=0$. Consequently, it follows that

$$R^*=\kappa/V_p=\Delta^{\sigma}l_c^2/(\tau_c V_p)\sim l_c\Delta^{\sigma-\gamma} \text{ as } \Delta\to 0 \ . \tag{10}$$

Thus, for consistency with $N^*\sim l_c^2\Delta^{-\phi}$, we require that $\sigma=(2\gamma-\phi)/2$, or $\sigma=(2-\phi)/2$, setting $\gamma=1$, which in either case gives $\sigma>0$ if $h<\infty$. Thus, our results for the divergence of the N^* show clearly that the kinetic surface tension between coexisting states vanishes at the transition (for $h<\infty$) and, in fact, provides a precise characterization of this behavior. This is quite different from equilibrium behavior, but not unprecedented for reaction systems [37] as noted in Sec. V.

TABLE IV. CC-ensemble estimates of y_A values for various critical sizes $N^*=L^2(1-\theta_A^*)$, chosen as the number of non-A sites. Note that one obtains $\phi\approx 1.65$ for $h=\frac{9}{4}$ using $y_2=0.5739$ augmenting the results in Table I.

		$h=0$		
N^*	$128^2\times 0.2=3277$	$128^2\times 0.1=1638$	$64^2\times 0.1=410$	$32^2\times 0.1=102$
y_A	0.5242	0.5232	0.5191	0.5064
		$h=\frac{3}{8}$		
N^*	$100^2\times 0.2=2000$	$64^2\times 0.2=819$	$64^2\times 0.08=328$	$32^2\times 0.1=102$
y_A	0.5483	0.5455	0.5395	0.5192
		$h=1$		
N^*	$164^2\times 0.15=4034$	$100^2\times 0.25=2500$	$64^2\times 0.1=410$	$32^2\times 0.15=154$
y_A	0.5606	0.5592	0.5470	0.5246
		$h=\frac{9}{4}$		
N^*	$164^2\times 0.15=4034$	$100^2\times 0.25=2500$	$64^2\times 0.108=442$	$64^2\times 0.06=246$
y_A	0.5672	0.5652	0.5467	0.5285
		$h=4$		
N^*	$164^2\times 0.26=6993$	$100^2\times 0.255=2550$	$100^2\times 0.2=2000$	$64^2\times 0.2=819$
y_A	0.5728	0.5675	0.5658	0.5545

TABLE V. Interpolated CC-ensemble data showing the dependence of the critical size N^* on h.

h \ Δ	0.03	0.0175	0.0066	0.0040
0		115	402	805
$\frac{3}{8}$	114	210	840	1920
1	190	410	1790	3880
4	630	1320	6990	

Note that consideration of the behavior of κ is generally complicated by the fact that its value (for fixed Δ) increases with the length scale l of observation [34]. For the above nucleation studies, one might set [39] $l \sim R^*$, so this effect alone would lead to an increase in κ as $\Delta \to 0$. However, the above results show that any such effect is dominated by an intrinsic decrease in κ as $\Delta \to 0$.

Finally, we elucidate the limiting $h \to \infty$ mean-field behavior mentioned above. In this limit, evolution of the reactive nucleus is described by the appropriate reaction-diffusion equations naturally cast in a cylindrical coordinate system [11] (see Appendix C). It follows immediately as a direct consequence of the form of the Laplacian diffusion operator in a curvilinear coordinate system that the influence of curvature on interface propagation velocity is described by [11]

$$V_p - V(R) \sim h/R \text{ for large } R \gg h^{1/2} \tag{11}$$

and, consequently, $R^* \approx h/V_p$ or $N^* \approx \pi(h/V_p)^2$. Since $V_p \sim h^{1/2}\Delta$ as $\Delta \to 0$ (so $\gamma = 1$), it follows that $N^* \sim h\Delta^{-2}$ as $\Delta \to 0$ and, thus, $\phi(h \to \infty) = 2$. It is also interesting to note that since the reaction-diffusion equations produce the same form for $V(R)$ versus R as obtained from consideration of the stochastic evolution equation for general h, we can identify the kinetic surface tension κ with h as $h \to \infty$.

VIII. NUCLEATION PHENOMENA: GROWTH PROBABILITY VERSUS PATCH SIZE

For a more complete characterization of the nucleation phenomena examined in Sec. VII, it is appropriate to consider the full dependence of the growth probability P_g of the reactive or empty patch embedded in the A-poisoned background on the initial patch size N. For example, Fig. 9(a) shows the behavior of P_g versus N for $h = 0$ and various y_A or Δ. Clearly, P_g increases more slowly with N as one approaches the transition (i.e., as $\Delta \to 0$), corresponding to the increasing critical size. It is thus more natural to consider P_g versus N/N^*, as shown in Fig. 9(b). More generally, here we shall analyze changes in the dependence of P_g on N/N^*, both in the limit as $\Delta \to 0$ (at fixed h) and also in the limit as $h \to \infty$ (at fixed Δ).

To this end, we propose the approximate, but general, scaling form

$$P_g \sim G[(N/N^* - 1)/\sigma(N^*)] \text{ for } N/N^* = O(1) , \tag{12}$$

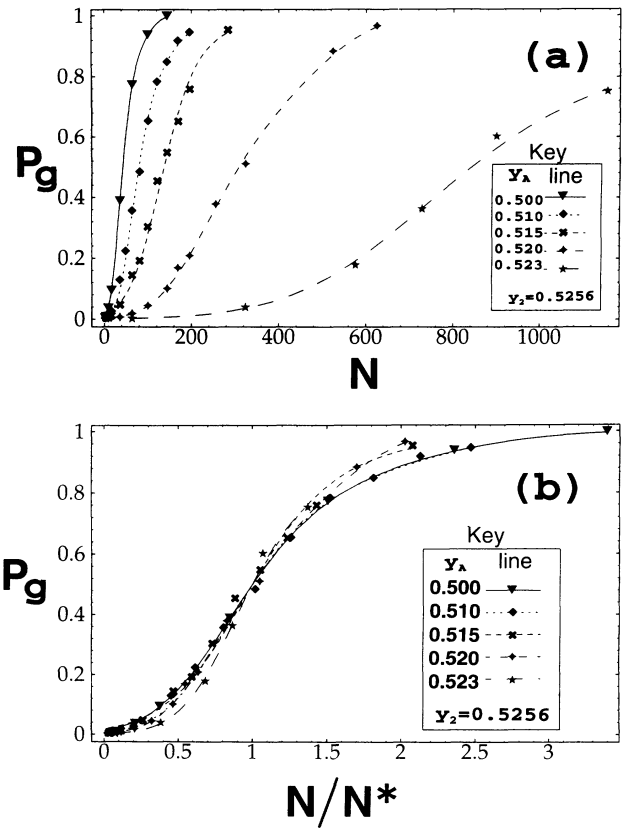

FIG. 9. (a) P_g vs N for various y_A when $h = 0$; (b) the same data replotted as P_g vs N/N^*.

where $G(0) = \frac{1}{2}$, $G(x) \to 0$ as $x \to -\infty$, and $G(x) \to 1$ as $x \to \infty$. The parameter σ measures the "width" of the transition region in P_g from 0 to 1, or the degree of smoothing of P_g from the step-function form $P_g = H(N/N^* - 1)$. Here $H(x) = 0(1)$ for $x < 0$ ($x > 0$). The latter is characteristic of the deterministic mean-field limit (where $\sigma \to 0$). From another perspective, $\delta N \sim N^*\sigma$ measures the degree of uncertainty, or "fuzziness," in the critical size.

Our *key proposition* is that the degree of fuzziness in the critical size (i.e., the magnitude of σ) is controlled by the size of the fluctuations at the perimeter of the critical nucleus. More specifically, let $\delta R \sim \delta(N^{1/2}) \sim (N^*)^{-1/2}\delta N \sim (N^*)^{1/2}\sigma \sim R^*\sigma$ denote the uncertainty in the critical radius, i.e., the range of R for which P_g differs significantly from 0 or 1. Then one expects that $\delta R \sim R^*\sigma$ roughly equals the fluctuation length $\xi = (\xi_i^2 + \xi_0^2)^{1/2}$ if $\xi < R^*$, or that δR roughly equals R^* itself if $R^* < \xi$ (fluctuations dominate). This implies that

$$\sigma \sim \min(1, \xi/R^*) . \tag{13}$$

We first apply these ideas to elucidate the behavior of P_g versus N/N^* as $\Delta \to 0$ (i.e., approaching the transition) for fixed h. Consider first the case $h = 0$ already shown in Fig. 9(b). Recall that here there are large intrinsic fluctuations $\xi_i \approx 20$ (lattice vectors) and that $\xi > \xi_i$. Now, since $R^* \leq 16$ for $\Delta \geq 0.005$ from Tables III–V, it

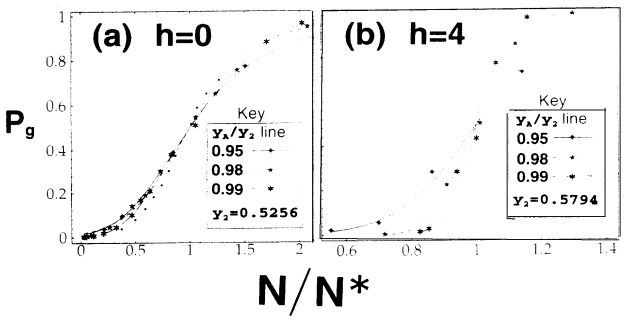

FIG. 10. Growth probability P_g vs N/N^* for $y_A/y_2=0.95$, 0.98, 0.99 when (a) $h=0$, (b) $h=4$. Significant sharpening as $y_A/y_2\to 1$ is only evident in this range for (b). Thus, we include additional data for $y_A/y_2=0.995$ (dotted line) in (a) to demonstrate asymptotic sharpening trend as $y_A/y_2\to 1$ (or $\Delta\to 0$).

follows that $\sigma=1$ in this range, explaining the collapse of corresponding curves and lack of sharpening in Fig. 9(b). Indeed, this previously observed lack of sharpening [16] was used to obtain an independent estimate of ϕ for $h=0$ (see Ref. [40]). However, as $\Delta\to 0$, eventually R^* must dominate ξ, at which point σ will start to decrease. The onset of this sharpening only occurs around $\Delta=0.0025$ [see Fig. 10(a)], where $R^*>20$ (see Tables III–V) exceeds ξ_i, and ξ_0 is still relatively small. In contrast, significant sharpening of P_g is observed for $h=4$ with decreasing Δ over the much broader range $\Delta\le 0.03$ [see Fig. 10(b)], since here $R^*\ge 14$ (Tables III–V) dominates both ξ_i and ξ_0, and thus ξ.

To determine the asymptotic behavior of σ, as $\Delta\to 0$, where $R^*\to\infty$ and $\xi\sim\xi_0$, one can utilize the scaling relation for ξ_0 described in Sec. V. For the circular geometry of relevance here, one must set $t\sim L\sim R$, and using $z>1$, one then obtains $\xi_0=\xi_0(R)\sim R^\beta$. For fixed $\Delta>0$, one would use the KPZ value of β. However, since we are interested in the limit as $\Delta\to 0$, where the KPZ nonlinearity and kinetic surface tension vanish, it is instead necessary to use the corresponding limiting value of β, namely, $\beta^*\approx 0.3$. One concludes that $\sigma\sim\xi_0(R^*)/R^*\sim\Delta^{(1-\beta^*)\phi/2}$, as $\Delta\to 0$. However, as a practical matter, this relation will be obscured by the presence of intrinsic fluctuations, and also by crossover effects as $\Delta\to 0$.

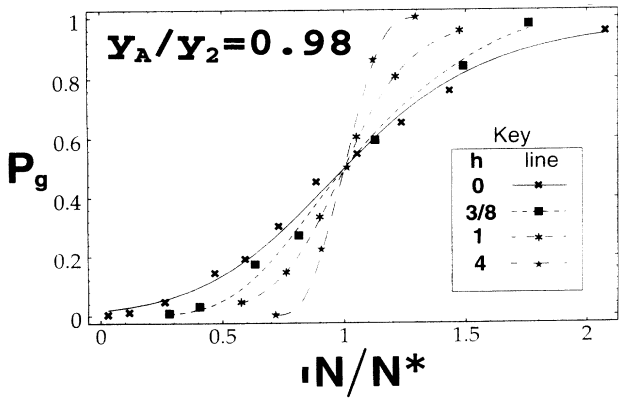

FIG. 11. Growth probability P_g vs N/N^* for $h=0$, $\frac{3}{8}$, 1, 4 (shown) at fixed $y_A/y_2=0.98$.

Finally, we demonstrate in Fig. 11 the dramatic convergence of P_g versus N/N^* to the deterministic step-function form $H(N/N^*-1)$, in the mean-field limit $h\to\infty$. Here, we have fixed Δ or, actually, y_A/y_2. The corresponding rapid decrease of $\sigma(h)=\xi(h)/R^*(h)$ is readily understood, since the intrinsic component $\xi_i(h)$ of $\xi(h)$ is rapidly quenched as h becomes nonzero, and $R^*(h)\sim h^{1/2}$ rapidly increases with h. The 50% decrease of σ as h increases from 1 to 4, so $\sigma\sim h^{-1/2}$, is consistent with roughly constant ξ in the above formula. This is reasonable for this h range, but we expect that the asymptotic decrease will be slower.

IX. CONCLUSIONS

In summary, we have provided a detailed and unified analysis of interface propagation and nucleation phenomena below the discontinuous monomer poisoning transition in the monomer-dimer surface reaction model with adspecies diffusion. Precise definition and treatment of propagation velocities and nucleus growth probabilities are only possible here because the transition is to an adsorbing state. This contrasts the situation for discontinuous transitions in equilibrium systems at nonzero temperatures. We show that interface propagation is described by the KPZ equation below the transition, with the KPZ nonlinearity, as well as the kinetic surface tension, vanishing approaching the transition. These observations are essential in elucidating the divergence of the critical nucleus size approaching the transition. The sharpening of the critical size approaching the transition (and with increasing adspecies diffusion rates) is also elucidated through a characterization of fluctuations at the interface between reactive and poisoned states. In this contribution, we have also succeeded in providing a unifying framework that can describe both the fluctuation-dominated behavior of the lattice-gas model for low adspecies diffusion rates and crossover to the deterministic mean-field behavior for high diffusion rates.

All of the concepts and ideas developed here should apply more generally for models incorporating discontinuous transitions to adsorbing states. These include more realistic models for CO oxidation [4], where the presence of the dimer species (oxygen) does not completely inhibit the adsorption of the monomer species (CO). We suggest, however, that their inclusion of cooperativity into the adsorption mechanism, or of interactions between the adspecies, would generally result in the kinetic surface tension of the reactive interface not vanishing at the transition (cf. Ref. [37]). Also, we note that the introduction of nonreactive desorption means that the transition is no longer to a trivial poisoned state, and the precise treatment of interface propagation and nucleus growth probabilities no longer applies. We are currently exploring these issues.

ACKNOWLEDGMENTS

Ames Laboratory is operated for the U.S. Department of Energy by Iowa State University under Contract No. W-7405-Eng-82. This work was supported by the

Division of Chemical Sciences, Office of Basic Energy Sciences. J.W.E. acknowledges valuable discussions with R. M. Ziff.

APPENDIX A: THE CC ENSEMBLE AND DETERMINATION OF CRITICAL SIZES

Simulation in the CC ensemble [24] at some fixed value θ_A^* of θ_A differs from conventional simulations only in the adsorption component of the algorithm. Instead of adsorbing different species with fixed relative rates, one attempts to deposit A if $\theta_A < \theta_A^*$ and B_2 if $\theta_A > \theta_A^*$, and measures the *asymptotic* value y_A^* of the fraction of attempts to deposit A. For an *infinite* system, (y_A^*, θ_A^*) should correspond to steady-state values in the conventional (constant pressure) ensemble, and so $y_A^* = y_2$ for the entire coexistence line $\theta_m < \theta_A^* < 1$. Here, θ_m is the limiting steady-state value of θ_A as $y_A \to y_2$ from below. However, this behavior is modified by finite-size effects in a way we exploit here.

For a finite $L \times L$ system (with periodic boundary conditions), if $\theta_A = \theta_A^*$ is chosen around $\frac{1}{2}$, then the CC ensemble selects a state where a linear strip of the A-poisoned state coexists with a reactive strip. However, for sufficiently high θ_A^*, the $L^2(1-\theta_A^*)$ non-A sites cannot form a stable percolating reactive strip. Then one or more nonpercolating reactive blobs will be formed and y_A will be selected to ensure that a blob of the mean size has an equal chance of growth or shrinkage, thus maintaining θ_A. As the system evolves, smaller blobs will occasionally shrink and disappear and the current y_A will increase to accommodate the larger mean blob size and corresponding lower mean radius of curvature. This process will continue until just one blob remains and $y_A \to y_A^*$ will correspond to an equal chance of growth or shrinkage for that blob of $N^*(y_A^*) = N = L^2(1-\theta_A^*)$ non-A sites. Thus, $N^*(y_A^*)$ is the critical size corresponding to y_A^*. Although this relationship appears to map out a middle unstable branch of the phase diagram (see Ref. [24]), clearly this branch depends on L, i.e., $1-\theta_A^* \sim O(L^{-2})$, as $L \to \infty$, for fixed y_A^*, and thus $N^*(y_A)$.

APPENDIX B: SPATIAL CONTACT AND DIFFUSION PROCESSES

A simple paradigm for the reaction model considered here is a "contact birth process" on a discrete space [10], augmented by diffusion of species at rate h. Let $p(l)$ denote the probability that a new species is born separated from its parent by l. We set $\sum_l p(l) = 1$, $\sum_l l p(l) = 0$, and $\sum_l l^2 p(l) = l_r^2$, so l_r denotes the characteristic contact or "reaction" range. Also, let b denote the total birth rate. Then the concentration or population $c(\mathrm{i})$, of species at site i satisfies

$$(d/dt)c(\mathrm{i}) = b\sum_l p(l)c(\mathrm{i}+l) + h\,\Delta c(\mathrm{i}) , \tag{B1}$$

where Δ denotes the discrete Laplacian. Assuming $c(\mathrm{i})$ is slowly varying in space, one expands $c(\mathrm{i}+l)$ about i and, retaining only terms to quadratic order (the diffusion approximation [10]), obtains

$$(d/dt)c(\mathrm{i}) \approx bc(\mathrm{i}) + (\tfrac{1}{2}bl_r^2 + h)\Delta c(\mathrm{i}) . \tag{B2}$$

Finally, after taking the spatial continuum limit, a trivial change of variable shows that characteristic lengths and, therefore, propagation velocities scale like $(\frac{1}{2}bl_r^2 + h)^{1/2}$.

To better mimic the reaction model of interest, one should include nonlinearity in the birth or reaction term, consider coupled equations for different species (as in general deterministic epidemic models [10]), and, finally, go beyond the mean-field description to treat spatial correlations. Any of these changes preclude simple analysis as above, but one expects characteristic lengths and velocities to still approximately scale as a root-mean-square sum of contributions from the reaction range and the diffusion length.

APPENDIX C: MEAN-FIELD REACTION-DIFFUSION EQUATIONS

Consider general lattice-gas reaction models involving two adspecies A and B that hop with rate h to adjacent empty sites, in the regime $h \to \infty$. Here the adlayer is well mixed, or "randomized," and evolution is described on the "macroscopic" diffusion length scale of $O(h^{1/2})$ lattice vectors by appropriate mean-field (MF) reaction-diffusion equations. These have the form [17]

$$\partial\theta_J/\partial t = R_J(\theta_A, \theta_B) + D\nabla^2\theta_J + D(\theta_J\nabla^2\theta_{J'} - \theta_{J'}\nabla^2\theta_J) , \tag{C1}$$

with $\{J, J'\} = \{A, B\}$, where the R_J describe the reaction mechanism, $D = a^2 h$ is the diffusion coefficient (for lattice constant a), and the nonlinear corrections to the Laplacian diffusion terms describe the interference of the presence of one species on the diffusion of the other (due to site blocking). In the limiting case of infinite reaction rate considered here, both species cannot exist at the same macroscopic point on the surface, and these nonlinear terms drop out [8].

Choosing R_J appropriate to the monomer-dimer reaction, one finds a bistability region where both reactive and A-poisoned states exist. One can monitor the evolution of the interface between these states using the above equations. For a planar interface, we previously showed that the propagation velocity satisfies [8,17] $V_p(MF) = D^{1/2}A'(y_A)$, where $A'(y_A)$ passes through zero linearly with varying y_A at an equistability point $y_A = y_2$ $(h = \infty)$ listed in Table I. We have also used these equations to analyze the evolution of a circular region of the reactive state of radius R embedded in an A-poisoned background. Since the theory is deterministic, the patch will either survive (for $R > R^*$, say) or die (for $R < R^*$), thus unambiguously determining a critical radius, $R^*(MF)$. Specifically, we have determined the proportionality constant in the relationship $N^*(MF) = \pi(R^*)^2 = E'(y_A)D$. We find that R^* is accurately approximated by D/V_p (error $< 5\%$ for $y_A/y_2 > 0.95$), so $E' \approx \pi(A')^{-2}$. Connections with lattice-gas (LG) reaction model behavior for $h \to \infty$ in Secs. IV and VII were made noting $D \leftrightarrow a^2 h$, $V_p(MF) \leftrightarrow aV_p(\mathrm{LG})$, $N^*(MF) \leftrightarrow a^2 N^*(\mathrm{LG})$, and so $A' \leftrightarrow A$ and $E' \leftrightarrow E$. For more details, see Ref. [41].

[1] V. P. Zhadanov and B. Kasemo, Surf. Sci. Rep. **20**, 111 (1994).
[2] J. W. Evans and M. Sabella, in *Trends in Statistical Physics* (Research Trends, Trivandrum, India, 1994).
[3] R. Dickman, Int. J. Mod. Phys. C **4**, 271 (1993).
[4] R. Imbihl, Prog. Surf. Sci. **44**, 185 (1993); G. Ertl, Adv. Catal. **37**, 213 (1990).
[5] R. M. Ziff, E. Gulari, and Y. Barshad, Phys. Rev. Lett. **56**, 2553 (1986).
[6] I. Jensen and H. Fogedby, Phys. Rev. A **42**, 1969 (1990).
[7] J. Mai, W. von Niessen, and A. Blumen, J. Chem. Phys. **93**, 3685 (1990); L. V. Lutsevich, V. I. Elokhin, A. V. Myshlyavtsev, A. G. Usov, and G. S. Yablonskii, J. Catal. **132**, 302 (1991).
[8] J. W. Evans, J. Chem. Phys. **98**, 2463 (1993).
[9] J. D. Gunton and M. Droz, *Introduction to the Theory of Metastable and Unstable States* (Springer, Berlin, 1983); K. Kaski, K. Binder, and J. D. Gunton, Phys. Rev. B **29**, 3996 (1984).
[10] D. Mollison, J. R. Stat. Soc. B **39**, 283 (1977).
[11] A. S. Mikhailov, *Foundations of Synergetics I,* Springer Series in Synergetics Vol. 51 (Springer, Berlin, 1990).
[12] *Dynamics of Fractal Surfaces,* edited by F. Family and T. Vicsek (World Scientific, Singapore, 1991).
[13] M. Kardar, G. Parisi, and Y.-C. Zhang, Phys. Rev. Lett. **56**, 342 (1986).
[14] P. Grassberger and A. De La Torre, Ann. Phys. **122**, 373 (1979).
[15] I. Jensen, H. C. Fogedby, and R. Dickman, Phys. Rev. A **41**, 3411 (1990).
[16] J. W. Evans and M. S. Miesch, Phys. Rev. Lett. **66**, 833 (1991).
[17] J. W. Evans, J. Chem. Phys. **97**, 572 (1992).
[18] B. J. Brosilow and R. M. Ziff, Phys. Rev. A **46**, 4534 (1992); E. V. Albano, Appl. Phys. A **54**, 2159 (1992); T. Tome and R. Dickman, Phys. Rev. E **47**, 948 (1993); J. W. Evans, Langmuir **7**, 2514 (1991).
[19] M. Dumont, P. Dufour, B. Sente, and R. Dagonnier, J. Catal. **122**, 95 (1990).
[20] M. Ehsasi, M. Matloch, O. Frank, J. H. Block, K. Christmann, F. S. Rys, and W. Hirschwald, J. Chem. Phys. **91**, 4949 (1989); H. P. Kaukonen and R. M. Nieminen, *ibid.* **91**, 4380 (1989).
[21] M. Tammaro, M. Sabella, and J. W. Evans (unpublished).
[22] P. Meakin and D. J. Scalapino, J. Chem. Phys. **87**, 731 (1987).
[23] D. G. Valchos, L. D. Schmidt, and R. Aris, Surf. Sci. **249**, 248 (1991).
[24] R. M. Ziff and B. J. Brosilow, Phys. Rev. A **46**, 4630 (1992).
[25] B. Chu, J. F. Schoenes, and M. F. Fisher, Phys. Rev. **185**, 219 (1969).
[26] J. W. Evans and M. S. Miesch, Surf. Sci. **245**, 401 (1991).
[27] For $h=\infty$, the mean-field rate equations yield $\theta_A \sim F_+[(y_A - y_{s+})(\exp\{y_A t\}-1)]$, where $y_{s+}=\frac{2}{3}$ and $F_+(x)=9x/(9x+2)$. However, the form $\theta_A \sim K_+[(y_A - y_{s+})t]$ works better for small h.
[28] R. Dickman, Phys. Rev. A **34**, 4246 (1986).
[29] J. Guckenheimer and P. Holmes, *Nonlinear Oscillations, Dynamical Systems and Bifurcations of Vector Fields* (Springer, New York, 1983).
[30] P. Fischer and U. Titulaer, Surf. Sci. **221**, 409 (1989).
[31] M. Eden, in *Proceedings of the Fourth Berkeley Symposium on Mathematical Statistics and Probability,* Berkeley, 1960, edited by J. Neyman (University of California Press, Berkeley, 1961).
[32] J. Kertesz and D. E. Wolf, J. Phys. A **21**, 747 (1988).
[33] H. C. Kang and J. W. Evans, Surf. Sci. **271**, 321 (1992).
[34] Dynamical renormalization group analysis indicates that $\kappa \sim l^{\alpha}$ depends on the length scale l of observation. See, e.g., C.-H. Lam and L. M. Sander, Phys. Rev. Lett. **71**, 561 (1993).
[35] J. Krug and P. Meakin, J. Phys. A **23**, L987 (1990).
[36] M. Tammaro and J. W. Evans (unpublished).
[37] H. C. Kang and W. H. Weinberg, Phys. Rev. E **47**, 1604 (1993).
[38] Similar refinement of previous η values (from Ref. [16]) is necessary for the monomer-dimer reaction with finite reaction rate k. For example, we find that η' is no greater than 0.6 for $k=1$.
[39] One might thus write $\kappa \sim \Delta^{\sigma'}(R^*)^{\alpha} l_c^2/\tau_c$, so then $\sigma'=\gamma-\frac{1}{2}\phi(1-\alpha)$.
[40] For $h=0$ and $\Delta \geq 0.005$, the relation $P_g \sim G(N/N^*-1)$ might have the form $P_g \sim (N/N^*)^{\chi}$, for $N \ll N^*$. Then $\chi=\nu\delta/\phi$ for consistency with $N^* \sim \Delta^{-\phi}$ and with $P_g \sim \Delta^{\nu\delta}$ (for fixed N). For $h=0$, we find that [16] $P_g \sim N^{2.5}$ for $N \ll N^*$ and fixed Δ, so $\phi=(\nu \approx 0.9)(\delta \approx 3.7)/(\chi \approx 2.5) \approx 1.3$, consistent with independent estimates for $h=0$ in Table I.
[41] T. R. Ray, Ph.D. thesis, Iowa State University, 1993.

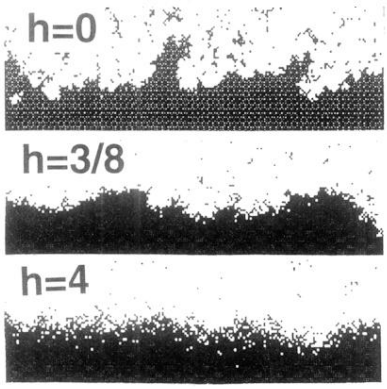

FIG. 4. Snapshots of a portion (200 lattice spacings wide) of the interface between reactive and poisoned states for $\Delta \approx 0$ and for various h. Only A-filled sites are shown.

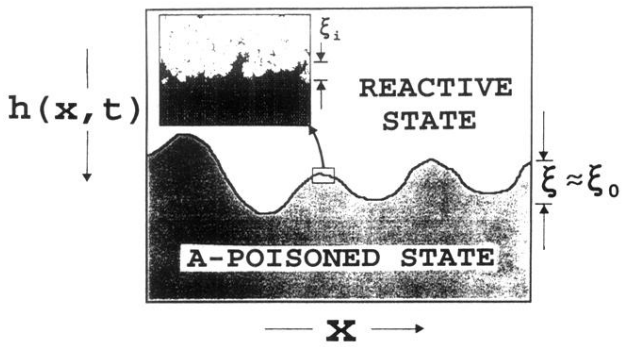

FIG. 6. Schematic of fluctuations in a coarse-grained picture of reactive interface evolution.